



# Tandem nanocatalyst design: putting two step-reaction sites into one location towards enhanced hydrogen transfer reactions

Yang You<sup>1†</sup>, Hao Huang<sup>1†</sup>, Keke Mao<sup>2†</sup>, Song Xia<sup>1</sup>, Di Wu<sup>1</sup>, Canyu Hu<sup>1</sup>, Chao Gao<sup>1</sup>, Panyiming Liu<sup>1</sup>, Ran Long<sup>1\*</sup>, Xiaojun Wu<sup>1</sup> and Yujie Xiong<sup>1\*</sup>

**ABSTRACT** Efficient tandem reactions on a single catalytic nanostructure would be beneficial to improving chemical transformation efficiency and reducing safety implications. It is imperative to identify the active sites for each single step reaction so that the entire reaction process can be optimized by designing and integrating the sites. Herein, hydrogen transfer reaction is taken as a proof-of-concept demonstration to show that the spatial integration of active sites is important to the catalytic efficiency of the entire process in tandem reactions. We identified specific active sites (i.e., various sites at faces *versus* corners and edges) for formic acid decomposition and alkene/nitrobenzene hydrogenation—the two steps in hydrogen transfer reactions, by employing three different shapes of Pd nanocrystals in tunable sizes. The investigation reveals that the decomposition of formic acid occurs preferentially at the edge sites of cubic nanocrystal and the plane sites of octahedral/tetrahedral nanocrystals, while the hydrogenation takes place mainly at the edge sites of both cubic and octahedral/tetrahedral nanocrystals. The consistency of active edge sites during different step reactions enables cubic nanocrystals to exhibit a higher activity than octahedral nanocrystals in hydrogen transfer reactions, although octahedrons offer comparable activities to cubes in formic acid decomposition and hydrogenation reactions. Guided by these findings, we further improved the overall performance of tandem catalysis by specifically promoting the limiting step through nanocatalyst design. This work provides insights into the rational design of heterogeneous nanocatalysts in tandem reactions.

**Keywords:** hydrogen transfer reaction, palladium, tandem reaction, reactive site, hydrogenation

## INTRODUCTION

Hydrogenation is a class of important reactions extensively involved in many chemical processes [1]. Hydrogen gas (H<sub>2</sub>) has been widely used as a hydrogen source for hydrogenation; however, there are safety issues in the process of production, storage, transportation and chemical manufacturing due to the natural flammable property of H<sub>2</sub>. Moreover, the majority of commercially used hydrogen is produced through steam reforming from hydrocarbons at high temperatures (700–1,200 K) while the production of H<sub>2</sub> is a strong demand of hydrogen energy in the coming decades. Thus it is an ideal scheme to perform hydrogenation reactions without the need of H<sub>2</sub> [2,3]. Organic compounds, such as formic acid (HCOOH) as non-toxic liquid at room temperature, are promising candidates to replace H<sub>2</sub> in hydrogenation reactions if comparable activities can be achieved [4,5].

To employ HCOOH as a hydrogen source for hydrogenation, it is imperative to develop efficient catalysts for multistep reactions in the so-called “tandem catalysis” systems that have drawn much attention from the research community of catalysis. For instance, a tandem catalytic system has been reported that CeO<sub>2</sub>-Pt can catalyze methanol decomposition for producing CO and H<sub>2</sub> which subsequently serve as feed stocks for ethylene hydroformylation catalyzed by neighbored Pt-SiO<sub>2</sub> [6]. Such tandem catalysis reduces the complexity of reaction systems and improves the recycling efficiency of reactants as all the reaction steps can be accomplished in a single reactor. While tandem catalysis often integrates multiple

<sup>1</sup> Hefei National Laboratory for Physical Sciences at the Microscale, Collaborative Innovation Center of Chemistry for Energy Materials (iChEM), School of Chemistry and Materials Science, and National Synchrotron Radiation Laboratory, University of Science and Technology of China, Hefei 230026, China

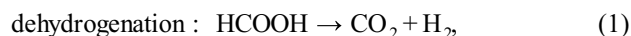
<sup>2</sup> School of Energy and Environment Science, Anhui University of Technology, Maanshan 243032, China

<sup>†</sup> These authors contributed equally to this paper.

\* Corresponding authors (emails: [yjxiong@ustc.edu.cn](mailto:yjxiong@ustc.edu.cn) (Xiong Y); [longran@ustc.edu.cn](mailto:longran@ustc.edu.cn) (Long R))

catalysts in a single system, the tandem reactions for the designated hydrogenation with HCOOH (i.e., hydrogen transfer through HCOOH decomposition and successive hydrogenation) may take place on a single catalytic nanostructure so that it becomes no longer necessary to implement multiple catalysts in a reaction system. Palladium (Pd)-based catalysts possess relatively high catalytic activities in organic couplings [7–9], oxidation [10], hydrogenation [11], and formic acid decomposition [12,13], which makes Pd nanocrystals become a suitable candidate for multistep tandem reactions [14–17].

Pd-based nanocatalysts are the most active materials for the decomposition of HCOOH, due to the lowest effective barrier [18]. The decomposition of HCOOH may follow two possible pathways [19]:



As the dehydrogenation process dominates the decomposition of HCOOH on Pd nanocatalysts [20], Pd-based nanocatalysts would enable HCOOH as an ideal hydrogen source for further hydrogenation. Such a hydrogen transfer scheme is a promising “green chemistry” approach to hydrogenation reactions [6,21].

In an ideal hydrogen transfer reaction, HCOOH is dehydrogenated to H atoms (adsorbed on catalyst,  $\text{H}_{\text{ad}}$ ) that can directly transfer to substrate molecules for hydrogenation before forming  $\text{H}_2$ . The reaction system does not have to go through the formation and dissociation of  $\text{H}_2$ , which will improve the reaction efficiency. To efficiently transfer  $\text{H}_{\text{ad}}$  atoms, the active sites for HCOOH dehydrogenation and substrate hydrogenation should be located together, while they are spatially separated in many cases. For this reason, the design of an efficient catalyst in multistep reactions relies on a clear determination of the real active sites for each single step. Previous reports have revealed the dependence of various reactions on structures including crystal planes, nanocrystal sizes and atomic sites [8,21–23]. For example, the semihydrogenation of alkyne mainly took place at the plane sites of Pd nanocrystals, while the overhydrogenation of alkyne and hydrogenation of alkene preferentially occurred at the edge sites [22]. Although tandem reactions are not involved in these reports, they provide the insights into the determination of active sites for a specific reaction.

Herein, we reveal the active sites for each single step in the hydrogen transfer reaction based on three types of uniform Pd nanocrystals with cubic, octahedral and tetrahedral shapes and different sizes. It turns out that the decomposition of HCOOH occurs preferentially at the

edge sites of cubic nanocrystals and the plane sites of octahedral/tetrahedral nanocrystals. Meanwhile, the hydrogenation of substrate molecules takes place mainly at the edge sites of both cubic and octahedral/tetrahedral nanocrystals. As such, the edge atoms of cubic nanocrystals become highly active sites for tandem hydrogen transfer reactions. Furthermore, we identify that the HCOOH decomposition is the limiting step in the tandem reaction. Guided by this result, we further improve the catalytic efficiency of entire hydrogen transfer reactions through promoting the HCOOH dehydrogenation with Ag-modified Pd catalysts. This work demonstrates the synergism between active sites in multistep tandem reactions and provides useful information for further heterogeneous catalyst design.

## EXPERIMENTAL SECTION

### First-principles simulations

All calculations based on spin polarized density functional theory (DFT) were performed by Vienna *ab initio* simulation package (VASP) [24]. Perdew-Burke-Ernzerhof of generalized gradient approximation (PBE-GGA) was employed in all calculations [24]. A plane wave cutoff of 400 eV was used with Gamma centered grid  $2 \times 2 \times 1$  for optimization and energy calculation. All atomic positions were optimized with the conjugate gradient method. The energy convergence was  $10^{-5}$  eV and the forces convergence was  $0.04 \text{ eV } \text{\AA}^{-1}$ . The optimized lattice constant of face-centered cubic Pd was 3.954 Å. In our calculation, the slab models for Pd {111} and Pd {100} surface consisted of 4-layer  $4 \times 4$  supercell containing 64 Pd atoms. In order to describe the step surface, a 5-layer  $3 \times 4$  rectangle supercell slab model was adopted with partial atoms of the top three layers removed. At the same time, Pd (100) step surface was simulated using a 5-layer  $3 \times 3$  supercell of rectangular  $\sqrt{2} \times \sqrt{2}$  unit cell model with partial atoms of the top three layers removed.

### Catalytic hydrogen transfer reaction measurement

The measurement was performed using an ordinary cuvette. The total volume of the reactor was about 20 mL. 0.2 mg Pd catalysts, 3 mmol HCOOH and 0.2 mmol substrate molecules were dispersed in 1 mL  $\text{H}_2\text{O}$  at room temperature without further operation. The reactor was sealed and heated at 50°C for 1 h. The amounts of substrates and products were determined using a gas chromatography-mass spectrometry (GC-MS, 7890A and 5975C, Agilent). The amount of HCOOH was determined using a Bruker AVANCE AV400 nuclear

magnetic resonance (NMR) spectrometer

## RESULTS AND DISCUSSION

Three types of uniform Pd nanocrystals with cubic (in three different sizes), octahedral (in two different sizes) and tetrahedral shapes as model catalysts were employed in the investigation. Here, the particle sizes are limited by the synthetic methods of Pd nanocrystals. Their catalytic activities can be evaluated for two step reactions (i.e., HCOOH decomposition, and substrate hydrogenation) and multistep hydrogen transfer reaction. To assess the performance of active sites, we employed a simple model to differentiate atomic sites, which involves four different types of atomic sites—cubic plane atoms,  $100_{\text{plane}}$  site; cubic edge atoms,  $100_{\text{edge}}$  site; octahedral/tetrahedral plane atoms,  $111_{\text{plane}}$  site; and octahedral/tetrahedral edge atoms,  $111_{\text{edge}}$  site (Fig. 1) [22]. As octahedral and tetrahedral shapes share the same atomic arrangement at the plane and edge sites, we classified them into a single type.

We first synthesized the Pd nanocrystals with three basic geometric shapes (cubes, octahedrons and tetrahedrons) covered by  $\{100\}$  or  $\{111\}$  facets, respectively (Figs S1–S3) [16,25], offering four different types of plane and edge atoms as illustrated in Fig. 1. Transmission electron microscopy (TEM) and high-resolution TEM (HRTEM) images (Figs S1, S2) show that the obtained Pd nanocrystals have cubic and octahedral/tetrahedral shapes mainly enclosed by  $\{100\}$  and  $\{111\}$  facets, respectively. By tuning their particle sizes (see Fig. S3 for size distribution diagrams), the nanocrystals with three different shapes can establish a platform allowing different types of plane and edge atoms. According to the statistics method in the literature (Table S1) [26], the percentages of edge atoms and plane atoms for the three types of nanocrystals are shown in Table S2. The statistics of surface atoms for ideal face-centered cubic (fcc) crystals are necessary to determine the numbers of different types of atoms (plane, edge or body atoms) on a nanocrystal with a given particle size and geometric shape. These three types of well-defined nanocrystals provide simple model systems to tune surface facets and edge-to-volume or plane-to-volume atomic ratios. To simplify the case, the “edge atoms” include the ones at the edges and corners, while the “plane atoms” denote the ones located on the faces of a polyhedron but exclude the ones at the edges and corners.

Once the types and amounts of surface atoms are defined, the catalytic activity from each type of sites in the step reactions and tandem reaction will be investigated. To explore the reaction mechanisms and identify the real

active sites, we employed several reactions to evaluate the performance of atomic sites. Fig. 2 outlines the relationship between tandem reaction and step reactions. In the presence of Pd catalysts, HCOOH can decompose into  $\text{H}_2$  and  $\text{CO}_2$  through the formation of  $\text{H}_{\text{ad}}$  atoms. With the same Pd catalysts, the hydrogenation of substrate molecules can be achieved with  $\text{H}_2$ , which undergoes the dissociation of  $\text{H}_2$  into  $\text{H}_{\text{ad}}$  atoms. With the two reactions taken together, Pd nanocrystals should be capable of catalyzing hydrogen transfer reactions directly through the intermediate of  $\text{H}_{\text{ad}}$ .

As both HCOOH decomposition and substrate hydrogenation have been reported as structure-sensitive reactions, the overall performance of hydrogen transfer reactions should depend on the types of active sites. In this study, the Pd nanocrystals shown in Figs S1, S2 are used for the evaluation in catalytic reactions. In order to evaluate the specific contribution of atomic sites to each step reaction, four types of atomic sites— $100_{\text{plane}}$  site,  $100_{\text{edge}}$  site,  $111_{\text{plane}}$  site and  $111_{\text{edge}}$  site are specified. In the analysis, all the surface atoms are considered to offer catalytic activity. To differentiate the contribution from different types of surface atoms, a model was employed to describe the observed experimental results as follow [22]:

$$\text{TOF}_{\text{surface}} = \text{TOF}_{\text{plane}} \cdot \gamma_{\text{plane}} + \text{TOF}_{\text{edge}} \cdot \gamma_{\text{edge}} \quad (3)$$

Here TOF is the experimental turnover frequency based on all the surface atoms of cubes/octahedrons/tetrahedrons, which depends on the percentage of each atom

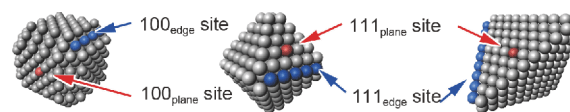


**Figure 1** Four different types of atomic sites on the nanocrystals used in this work.

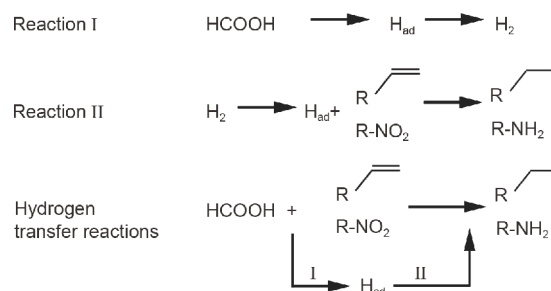


**Figure 2** Relationship between tandem reactions and step reactions based on multifunctional Pd catalyst. Reaction I is HCOOH decomposition to  $\text{H}_2$ , reaction II is hydrogenation reaction by molecular  $\text{H}_2$ , and tandem reaction is a one-pot hydrogen transfer reaction for hydrogenation by HCOOH.

type ( $\gamma_i$ ) and its specific activity (TOF<sub>*i*</sub>). The implementation of the model to the samples allows us to estimate the reaction activity of four types of surface atoms in catalytic reactions.

The process for determining active sites starts with reaction I (decomposition of HCOOH, reaction setup shown in Fig. S4) using the six model catalysts mentioned above. Table 1 shows the catalytic performance of samples under the same reaction condition. The TOF for each sample was determined based on the experimentally observed production of H<sub>2</sub> and CO<sub>2</sub>. According to the method in the literature [22], the analysis model was first applied to the cubic nanocrystals with three sizes. Since the cubic nanocrystals with three sizes are all enclosed by {100} facets, the only difference between these samples is the variety of  $\gamma_{\text{edge}}$  and  $\gamma_{\text{surface}}$ . The formula ( $\text{TOF}_{\text{surface}} = \text{TOF}_{\text{plane}} \cdot \gamma_{\text{plane}} + \text{TOF}_{\text{edge}} \cdot \gamma_{\text{edge}}$ ) is firstly applied with the statistics of surface atoms from Table S2 to estimate TOF<sub>100<sub>plane</sub></sub> and TOF<sub>100<sub>edge</sub></sub>. Based on the calculation results, the 100<sub>edge</sub> sites show a dramatically higher activity in catalytic HCOOH decomposition. Meanwhile, we analyzed the three samples of octahedral and tetrahedral nanocrystals with the same {111} facets to estimate TOF<sub>111<sub>plane</sub></sub> and TOF<sub>111<sub>edge</sub></sub>. The calculation results indicate that Pd 111<sub>plane</sub> sites make a major contribution to the catalytic activity of octahedrons and tetrahedrons in HCOOH decomposition, and they are significantly more active than the plane atoms of cubic nanocrystals. According to the TOFs, the edge atoms on cubic nanocrystals possess the highest catalytic activity in reaction I (HCOOH decomposition).

To further investigate the impact of capping ligands on catalytic performance, Fourier-transform infrared spectroscopy (FTIR) was employed to examine the surface ligands on the Pd nanocubes. As displayed in Fig. S5, most ligands such as polyvinyl pyrrolidone (PVP) have

been removed by the centrifugation and washing process. When the washed sample is further treated with water steam—a well-recognized extensive-cleaning method [27], no surface change can be observed. This indicates that our washing process provides the comparable clean surface to steam treatment. Moreover, the Pd nanocubes treated with the washing process exhibit consistent catalytic activities with those treated with steam treatment. This further confirms that the catalytic measurements are not affected by surface ligands. In our work, all the samples were washed for at least 6 times and thus maintained equally clean.

To gain insight into the HCOOH decomposition at various sites, we have employed first-principles simulation to calculate the reaction energy (Figs S6–S8). The simulation results show that the dehydrogenation takes place through five intermediate states: (1) the adsorption of HCOOH<sub>ad</sub>; (2) the dehydrogenation of the first H atom to form HCOO<sub>ad</sub> and H<sub>ad</sub>; (3) the first rotation step, namely HCOO<sub>ad</sub>+H<sub>ad</sub> (R<sub>1</sub>); (4) the second rotation step, namely HCOO<sub>ad</sub>+H<sub>ad</sub> (R<sub>2</sub>); and (5) the dehydrogenation of the second H atom to form CO<sub>2</sub> and 2H<sub>ad</sub>. As displayed in Fig. S9, the reaction energies at 100<sub>edge</sub> sites are relatively lower than those at the other three sites at the HCOO<sub>ad</sub>+H<sub>ad</sub> (R<sub>1</sub>) and HCOO<sub>ad</sub>+H<sub>ad</sub> (R<sub>2</sub>) stages. At the 100<sub>plane</sub>, 111<sub>edge</sub> and 111<sub>plane</sub> sites, a rotation process of Pd–O bonds requires more energy to overcome reaction barriers. In sharp contrast, this step at 100<sub>edge</sub> sites is accompanied with the formation of C–Pd bonds for bridged adsorption, leading to the reduced reaction energy. In this case, although the final states at 111<sub>plane</sub> sites and 100<sub>plane</sub> sites are at lower energy levels, the higher energy of intermediate steps limits their overall reaction rates (Fig. S9). These simulation results agree well with the experimental TOFs for HCOOH dehydrogenation reaction.

**Table 1** Activity model as applied to catalytic HCOOH decomposition occurring on differently shaped and sized Pd nanocrystals, which accounts for the structure sensitivity of HCOOH decomposition<sup>a</sup>

	Cube	Cube	Cube	Oct.	Oct.	Tetra.
Size (nm)	8.5±1.6	14.4±1.4	23.3±1.3	8.5±1.1	29.0±2.4	8.0±0.5
V (mL) <sup>b</sup>	8.1	2.7	1.4	19.1	5.9	33.2
TOF <sub>surface</sub> (h <sup>-1</sup> )	12.1	6.6	5.5	18.8	19.8	18.6
TOF <sub>100<sub>edge</sub></sub> (h <sup>-1</sup> )		222.0±36.1			–	
TOF <sub>100<sub>plane</sub></sub> (h <sup>-1</sup> )		1.7±0.8			–	
TOF <sub>111<sub>edge</sub></sub> (h <sup>-1</sup> )		–			4.8±3.2	
TOF <sub>111<sub>plane</sub></sub> (h <sup>-1</sup> )		–			20.1±0.4	

a) Reaction conditions: 1 mol L<sup>-1</sup> HCOOH aqueous solution (10 mL), 12.5 mg Pd nanocrystals, 120 min, 365 K. The volume of H<sub>2</sub> and CO<sub>2</sub> is measured by gas burette. No CO is observed in GC. b) V, defined as the volume of produced H<sub>2</sub> and CO<sub>2</sub> gas.

We then looked into reaction II using the hydrogenation of styrene as a model reaction to evaluate the catalytic activities at various sites. Similar to the analysis for reaction I, the TOFs for four types of sites in reaction II (hydrogenation reaction) were determined based on their experimental reaction yields (Table 2). The calculated results show that the edge sites of both cubic and octahedral/tetrahedral nanocrystals are more catalytically active than their plane sites for styrene hydrogenation by  $H_2$ , regardless of their atomic arrangements. This finding agrees well with the previous reports that the high activity of edge atoms benefits from their low coordination number [19]. More specifically, the catalytic activity of  $100_{\text{edge}}$  sites is substantially higher than that of  $111_{\text{edge}}$  sites.

Upon the identification of the active sites in step reactions, we further investigated the tandem reaction (reaction I + reaction II) using the same catalysts. The tandem reaction was carried out in the presence of HCOOH, substrate molecules and Pd nanocrystals in argon or air atmosphere without the addition of molecular  $H_2$ . The measurement results show that the atmosphere of argon or air does not bring any difference to the yield of this tandem reaction. To confirm the origin of hydrogen in hydrogenation, we measured the  $H_2$  production accompanied with this tandem reaction. Taking 14.4 nm Pd cubic nanocrystals as example, the reaction system produces almost no  $H_2$  after reaction at 323 K for 60 min, significantly less than that in the absence of substrate molecules (3  $\mu\text{L}$ ). Nearly all the  $H_{\text{ad}}$  atoms from HCOOH decomposition has been consumed by the hydrogenation of styrene, demonstrating the success of tandem reaction. Furthermore, we also performed the tandem reaction under a slow argon flow (see Fig. S10). The argon flow can timely remove the produced  $H_2$  from the reaction system, which consumes  $H_{\text{ad}}$  for  $H_2$  pro-

duction by breaking  $H_{\text{ad}} \leftrightarrow H_2$  equilibrium. It turns out that the yield of product drops down to only 6% with an extremely slow Ar flow. This suggests that the tandem reaction, which is associated with the formation of  $H_{\text{ad}}$ , either competes with or relies on the release of  $H_2$ . To exclude the uncertainty of catalytic performance, we performed 5 parallel experiments for each reaction condition. In addition, the hydrogen transfer reaction with five-fold scale was performed under the same condition based on 14.4 nm Pd nanocubes, achieving the yield of 29.2% that is consistent with that by the small system.

Given the confirmation of tandem reaction, we implemented a similar analysis process in the tandem reaction to obtain the TOFs for four types of atomic sites (Table 3). Interestingly, the edge sites of Pd cubic nanocrystals show an unprecedentedly high TOF as compared with the other three types of atomic sites. We can thus conclude that a high TOF in the tandem reaction relies on the high catalytic activities in all the step reactions (Table S3). It is worth pointing out that the TOF of tandem reaction is dramatically higher than those of HCOOH decomposition and styrene hydrogenation with molecular  $H_2$  (Tables 1–3). This suggests that the tandem reaction can undergo a direct hydrogen transfer for hydrogenation without the forming and dissociating of  $H_2$ .

Based on the experimental results above, we can propose a mechanism for the tandem reaction that involves HCOOH decomposition and styrene hydrogenation. In the case of octahedral and tetrahedral nanocrystals (Fig. 3a), the decomposition of HCOOH preferentially takes place at their  $\{111\}$  plane atoms (step 1). These newly generated  $H_{\text{ad}}$  atoms can form molecular  $H_2$  (step 2), or further spillover to other locations such as edge sites (step 3). The involvement of  $H_{\text{ad}}$  diffusion over metal surface in hydrogenation has been systematically investigated [28–30]. It should be pointed out that the

**Table 2** Activity model as applied to catalytic styrene hydrogenation with molecular  $H_2$  occurring on differently shaped and sized Pd nanocrystals, which accounts for the structure sensitivity of styrene hydrogenation<sup>a</sup>

	Cube	Cube	Cube	Oct.	Oct.	Tetra.
Size (nm)	8.5±1.6	14.4±1.4	23.3±1.3	8.5±1.1	29.0±2.4	8.0±0.5
Yield (%)	51.5±8.1	29.0±4.2	17.6±5.6	43.3±6.8	12.0±4.5	76.1±7.1
TOF <sub>surface</sub> ( $\text{h}^{-1}$ )	403.8	372.5	360.2	223.8	212.0	224.2
TOF <sub>100<sub>edge</sub></sub> ( $\text{h}^{-1}$ )		1823.4±299.2			–	
TOF <sub>100<sub>plane</sub></sub> ( $\text{h}^{-1}$ )		333.6±8.3			–	
TOF <sub>111<sub>edge</sub></sub> ( $\text{h}^{-1}$ )		–			344.0±60.1	
TOF <sub>111<sub>plane</sub></sub> ( $\text{h}^{-1}$ )		–			211.6±6.0	

a) Reaction conditions: 0.2 mol  $L^{-1}$  styrene solution (1 mL), 0.2 mg Pd nanocrystals, 60 min, 323 K, 10%  $H_2$  in atmospheric pressure.

**Table 3** Activity model as applied to hydrogen transfer reaction occurring on differently shaped and sized Pd nanocrystals, which accounts for the structure sensitivity of the tandem reaction<sup>a</sup>

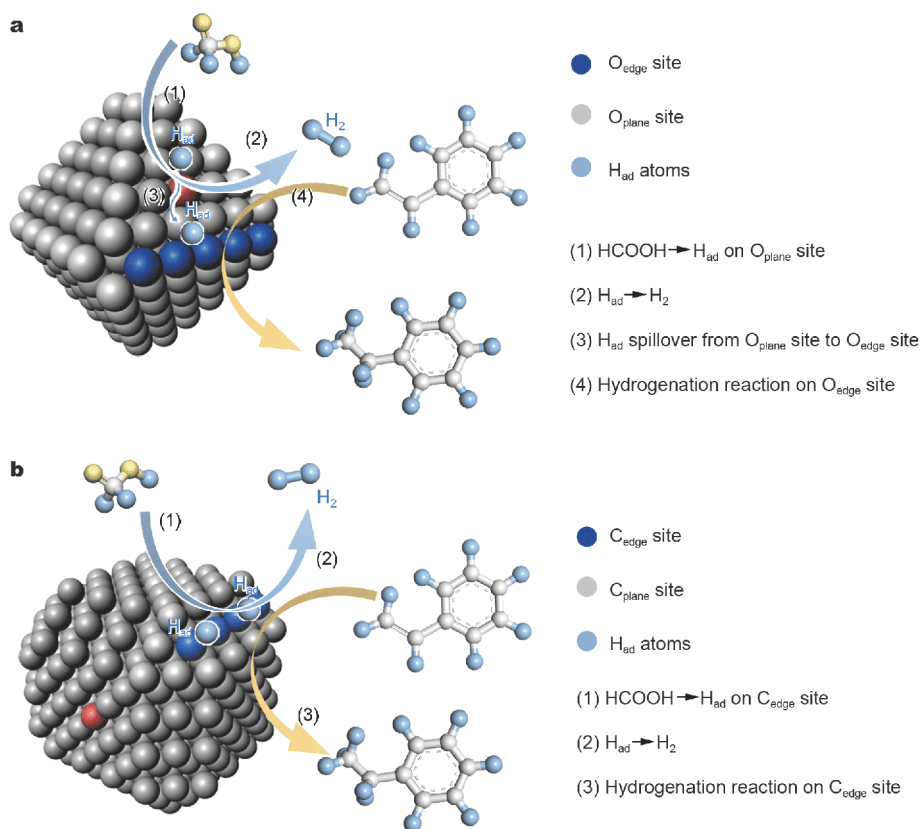
	Cube	Cube	Cube	Oct.	Oct.	Tetra.
Size (nm)	8.5±1.6	14.4±1.4	23.3±1.3	8.5±1.1	29.0±2.4	8.0±0.5
Yield (%)	75.6±0.8	30.2±1.1	13.8±1.0	49.5±0.3	14.1±0.4	89.9±2.6
TOF <sub>surface</sub> (h <sup>-1</sup> )	592.9	387.7	282.3	255.8	249.1	264.9
TOF100 <sub>edge</sub> (h <sup>-1</sup> )		10,936.0±574.1			–	
TOF100 <sub>plane</sub> (h <sup>-1</sup> )		98.7±15.9			–	
TOF111 <sub>edge</sub> (h <sup>-1</sup> )		–			534.4±156.1	
TOF111 <sub>plane</sub> (h <sup>-1</sup> )		–			231.6±15.7	

a) Reaction conditions: 0.2 mmol styrene solution (1 mL), 0.2 mg Pd nanocrystals, 3 mol L<sup>-1</sup> HCOOH aqueous solution (1 mL), 60 min, 323 K.

previous calculation results show that the mean free path of a single H atom on clean Pd {111} surface is much shorter than that on Pd {100} facets [29,30]. As the 111<sub>plane</sub> sites possess lower catalytic activity for hydrogenation than the 111<sub>edge</sub> sites as demonstrated in Table 2, most of the H<sub>ad</sub> atoms should produce H<sub>2</sub> on {111} planes during the spillover process (step 3). The H<sub>ad</sub> atoms reaching 111<sub>edge</sub> sites from step 3 can participate in hy-

drogenation reaction (step 4). Thus it is understandable that the octahedral and tetrahedral nanocrystals exhibit a relatively low TOF of octahedrons in the overall tandem reaction.

In comparison, the step reactions occurring on Pd cubic nanocrystals follow a different situation as illustrated in Fig. 3b. According to our TOF analysis, the dehydrogenation of HCOOH possesses a higher reaction rate

**Figure 3** Schematic illustration for the major steps involved in the tandem reaction: (a) Pd octahedral nanocrystal, and (b) Pd cubic nanocrystal.

at the edge sites of cubic nanocrystals, producing a large number of  $H_{ad}$  atoms around the  $100_{edge}$  sites. As  $H_{ad}$  atoms are preferentially generated at the  $100_{edge}$  sites which are very close to the favorable locations for the next hydrogenation step, the overall reactions can easily be carried out in a high TOF by shortening the path of  $H_{ad}$  spillover. From this view, the consistency of the active site locations for step reactions is the prerequisite for achieving a high TOF for tandem reactions. Even the  $H_{ad}$  atoms produced at  $100_{plane}$  sites can spillover to edge sites with a higher efficiency owing to the longer mean free path on Pd {100}. As such, the hydrogenation through hydrogen transfer scheme can more efficiently take place on Pd cubic nanocrystals. Based on the obtained results, we can conclude that in addition to the coordination effect [31], the spillover of  $H_{ad}$  atoms is also critical to the activity of tandem reactions.

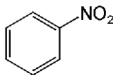
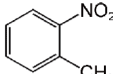
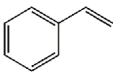
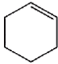
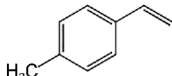
To verify the generic feature of tandem reaction, we investigated the substrate scope of the hydrogen transfer reaction with HCOOH as hydrogen source at 50°C under optimized conditions. In this scope, nitrobenzene and other alkene were chosen as substrates. The experimental results demonstrate that Pd nanocube is an effective catalyst for various hydrogen transfer reactions including the hydrogenation of C=C bond and  $-NO_2$  (Table 4). According to the TOFs of reaction I (decomposition of HCOOH, Table 1) and reaction II (hydrogenation reaction with molecular  $H_2$ , Table 2), we recognize that the

limitation for hydrogen transfer reactions originates from HCOOH decomposition. Previous work revealed that the HCOOH decomposition can be accelerated by bimetallic AgPd catalyst [32,33]. To further enhance the hydrogen transfer reactions, we employed the Ag-modified Pd nanocubes (Pd@Ag, Fig. S11) as catalyst. It is worth mentioning that the capping of {100} by  $Br^-$  enables the selective overgrowth of metallic atoms starting at the edges of Pd nanocubes [34]. In this case, the additional metallic atoms will spillover from edges to plane sites, forming the Pd nanocubes with both edge and plane sites modified by Ag atoms. As a result, the TOFs for all the reactions have been increased by such an Ag modification (Table 4). The Ag modification can accelerate the HCOOH decomposition, forming  $H_{ad}$  not only at edge sites but also on planes, both of which will promote the overall tandem reactions. Thus the identification of active sites in this work can serve as guidance for the future development of more efficient catalysts.

## CONCLUSIONS

We have developed a heterogeneous hydrogen transfer system for hydrogenation by using a promising hydrogen storage medium—formic acid. Leveraging this platform, we have examined the catalytic performance of Pd nanocatalysts based on the nanocrystals with basic geometrical shapes, and determined the real catalytically active sites for step reactions. This work reveals that putting two

**Table 4** Substrate scope of hydrogen transfer reactions using Pd nanocubes or Pd@Ag nanocubes (14.4 nm) as catalysts at the same Pd usage (0.2 mg)<sup>a</sup>

Entry	Substrate	HCOOH (mmol)	TOF with Pd ( $h^{-1}$ )	TOF with Pd@Ag ( $h^{-1}$ )
1		0.5	1064.2±34.2	1554.1±35.7
2		0.5	930.9±42.5	1,516.3±24.5
3		3	387.7±14.1	438.8±43.5
4		3	140.0±18.8	739.8±37.8
5		3	131.2±38.2	295.0±19.8

a) Reaction conditions: 0.2 mmol substrate (1 mL), 323 K, 1 h.

step-reaction sites into one location can dramatically enhance the overall efficiency of hydrogen transfer reactions, which provides an approach to further develop both cost-effective and highly efficient catalysts for organic reactions. Furthermore, the determination of real active sites identifies the limiting step for a tandem reaction, allowing us to further optimize the construction of catalysts. This concept would facilitate the practical application of HCOOH as a hydrogen storage/generation medium in the view of heterogeneous catalysis, and can potentially be extended to the rational catalyst design for other types of heterogeneous tandem reactions. Overall, the active sites on metal surface offer a knob at the atomic level for tuning the catalytic efficiency of metal nanomaterials, which is important to the design of more complex catalysts such as bimetallic or trimetallic nanocrystals.

Received 15 March 2019; accepted 03 April 2019;  
published online 23 April 2019

- 1 Symes MD, Cronin L. Decoupling hydrogen and oxygen evolution during electrolytic water splitting using an electron-coupled-proton buffer. *Nat Chem*, 2013, 5: 403–409
- 2 Yu C, Guo X, Xi Z, *et al.* AgPd nanoparticles deposited on WO<sub>2.72</sub> nanorods as an efficient catalyst for one-pot conversion of nitrophenol/nitroacetophenone into benzoxazole/quinazoline. *J Am Chem Soc*, 2017, 139: 5712–5715
- 3 Sorribes I, Wienhöfer G, Vicent C, *et al.* Chemoselective transfer hydrogenation to nitroarenes mediated by cubane-type Mo<sub>3</sub>S<sub>4</sub> cluster catalysts. *Angew Chem Int Ed*, 2012, 51: 7794–7798
- 4 Johnson TC, Morris DJ, Wills M. Hydrogen generation from formic acid and alcohols using homogeneous catalysts. *Chem Soc Rev*, 2010, 39: 81–88
- 5 Aldous L, Compton RG. Clean, efficient electrolysis of formic acid via formation of eutectic, ionic mixtures with ammonium formate. *Energy Environ Sci*, 2010, 3: 1587
- 6 Yamada Y, Tsung CK, Huang W, *et al.* Nanocrystal bilayer for tandem catalysis. *Nat Chem*, 2011, 3: 372–376
- 7 Collins G, Schmidt M, O'Dwyer C, *et al.* The origin of shape sensitivity in palladium-catalyzed Suzuki-Miyaura cross coupling reactions. *Angew Chem Int Ed*, 2014, 53: 4142–4145
- 8 Wu XF, Anbarasan P, Neumann H, *et al.* From noble metal to nobel prize: Palladium-catalyzed coupling reactions as key methods in organic synthesis. *Angew Chem Int Ed*, 2010, 49: 9047–9050
- 9 Long R, Wu D, Li Y, *et al.* Enhancing the catalytic efficiency of the Heck coupling reaction by forming 5 nm Pd octahedrons using kinetic control. *Nano Res*, 2015, 8: 2115–2123
- 10 Long R, Huang H, Li Y, *et al.* Palladium-based nanomaterials: A platform to produce reactive oxygen species for catalyzing oxidation reactions. *Adv Mater*, 2015, 27: 7025–7042
- 11 Kyriakou G, Boucher MB, Jewell AD, *et al.* Isolated metal atom geometries as a strategy for selective heterogeneous hydrogenations. *Science*, 2012, 335: 1209–1212
- 12 Cai YY, Li XH, Zhang YN, *et al.* Highly efficient dehydrogenation of formic acid over a palladium-nanoparticle-based mott-schottky photocatalyst. *Angew Chem Int Ed*, 2013, 52: 11822–11825
- 13 Zhang S, Metin Ö, Su D, *et al.* Monodisperse AgPd alloy nanoparticles and their superior catalysis for the dehydrogenation of formic acid. *Angew Chem Int Ed*, 2013, 52: 3681–3684
- 14 Shao M, Odell J, Humbert M, *et al.* Electrocatalysis on shape-controlled palladium nanocrystals: Oxygen reduction reaction and formic acid oxidation. *J Phys Chem C*, 2013, 117: 4172–4180
- 15 Huang X, Tang S, Mu X, *et al.* Freestanding palladium nanosheets with plasmonic and catalytic properties. *Nat Nanotech*, 2011, 6: 28–32
- 16 Long R, Mao K, Ye X, *et al.* Surface facet of palladium nanocrystals: A key parameter to the activation of molecular oxygen for organic catalysis and cancer treatment. *J Am Chem Soc*, 2013, 135: 3200–3207
- 17 Jiang K, Xu K, Zou S, *et al.* B-doped Pd catalyst: boosting room-temperature hydrogen production from formic acid–formate solutions. *J Am Chem Soc*, 2014, 136: 4861–4864
- 18 Luo Q, Feng G, Beller M, *et al.* Formic acid dehydrogenation on Ni(111) and comparison with Pd(111) and Pt(111). *J Phys Chem C*, 2012, 116: 4149–4156
- 19 Tedsree K, Li T, Jones S, *et al.* Hydrogen production from formic acid decomposition at room temperature using a Ag–Pd core–shell nanocatalyst. *Nat Nanotech*, 2011, 6: 302–307
- 20 Wang ZL, Yan JM, Ping Y, *et al.* An efficient CoAuPd/C catalyst for hydrogen generation from formic acid at room temperature. *Angew Chem Int Ed*, 2013, 52: 4406–4409
- 21 You Y, Huang H, Xia S, *et al.* Design of Pd{111}-TiO<sub>2</sub> interface for enhanced catalytic efficiency towards formic acid decomposition. *Sci China Chem*, 2018, 61: 1123–1127
- 22 Crespo-Quesada M, Yarulin A, Jin M, *et al.* Structure sensitivity of alkyne hydrogenation on shape- and size-controlled palladium nanocrystals: which sites are most active and selective? *J Am Chem Soc*, 2011, 133: 12787–12794
- 23 Long R, Mao K, Gong M, *et al.* Tunable oxygen activation for catalytic organic oxidation: Schottky junction versus plasmonic effects. *Angew Chem Int Ed*, 2014, 53: 3205–3209
- 24 Kresse G, Furthmüller J. Efficient iterative schemes for *ab initio* total-energy calculations using a plane-wave basis set. *Phys Rev B*, 1996, 54: 11169–11186
- 25 Li B, Long R, Zhong X, *et al.* Investigation of size-dependent plasmonic and catalytic properties of metallic nanocrystals enabled by size control with HCl oxidative etching. *Small*, 2012, 8: 1710–1716
- 26 Vanharde R, Hartog F. The statistics of surface atoms and surface sites on metal crystals. *Surf Sci*, 1969, 15: 189–230
- 27 Kar S, Sen R, Goeppert A, *et al.* Integrative CO<sub>2</sub> capture and hydrogenation to methanol with reusable catalyst and amine: toward a carbon neutral methanol economy. *J Am Chem Soc*, 2018, 140: 1580–1583
- 28 Liu D, Xie M, Wang C, *et al.* Pd-Ag alloy hollow nanostructures with interatomic charge polarization for enhanced electrocatalytic formic acid oxidation. *Nano Res*, 2016, 9: 1590–1599
- 29 Blanco-Rey M, Juaristi JL, Diez Muiño R, *et al.* Electronic friction dominates hydrogen hot-atom relaxation on Pd(100). *Phys Rev Lett*, 2014, 112: 103203
- 30 Dong W, Hafner J. H<sub>2</sub> dissociative adsorption on Pd(111). *Phys Rev B*, 1997, 56: 15396–15403
- 31 Wolff CM, Frischmann PD, Schulze M, *et al.* All-in-one visible-light-driven water splitting by combining nanoparticulate and molecular co-catalysts on CdS nanorods. *Nat Energy*, 2018, 3: 862–



869

- 32 Liu PYM, Cai Z, You Y, *et al.* Surface modification on Pd-TiO<sub>2</sub> hybrid nanostructures towards highly efficient H<sub>2</sub> production from catalytic formic acid decomposition. *Chem Eur J*, 2018, 24: 18398–18402
- 33 Tada H, Mitsui T, Kiyonaga T, *et al.* All-solid-state Z-scheme in CdS–Au–TiO<sub>2</sub> three-component nanojunction system. *Nat Mater*, 2006, 5: 782–786
- 34 Xie S, Lu N, Xie Z, *et al.* Synthesis of Pd-Rh core-frame concave nanocubes and their conversion to Rh cubic nanoframes by selective etching of the Pd cores. *Angew Chem Int Ed*, 2012, 51: 10266–10270

**Acknowledgements** This work was financially supported in part by the National Key R&D Program of China (2017YFA0207301), the National Natural Science Foundation of China (21725102, U1832156, 21601173, 21890751 and 21803002), CAS Key Research Program of Frontier Sciences (QYZDB-SSW-SLH018), CAS Interdisciplinary Innovation Team, the Ministry of Science and Technology of China (2016YFA0200602 and 2018YFA0208603), and the Chinese Universities Scientific Fund (WK2310000067). We thank the support from USTC Center for the Micro- and Nanoscale Research and Fabrication.

**Author contributions** Xiong Y and Long R conceived the research and designed the experiments. You Y and Huang H carried out the experiments. Mao K and Wu X contributed to the simulation. Xia S, Wu D, Hu C and Liu P contributed to the catalytic performance measurement. Gao C, Long R and Xiong Y wrote the manuscript with comments from the other authors. All authors contributed to the general discussion.

**Conflict of interest** The authors declare that they have no conflict of interest.

**Supplementary information** Experimental details and supporting data are available in the online version of the paper.



**Yang You** was born in Jiangxi, China, in 1991. He received his BSc degree in material chemistry in 2013 from the University of Science and Technology of China (USTC). Since then he has been studying as a PhD candidate under the tutelage of Professor Yujie Xiong at the USTC. His research interests focus on the controlled synthesis and catalytic applications of metal nanostructures.



**Ran Long** was born in Anhui, China, in 1987. She received her BSc in chemistry in 2009 and PhD in inorganic chemistry under the tutelage of Professor Yujie Xiong in 2014, both from the USTC. After postdoctoral training with Professors Yujie Xiong and Li Song, she is currently an associate professor working at the USTC. Her research interests focus on the controlled synthesis and catalytic applications of metal nanocrystals.



**Yujie Xiong** received his BSc in chemical physics in 2000 and PhD in inorganic chemistry in 2004, both from the USTC. After four-year postdoctoral training at the University of Washington in Seattle and the University of Illinois at Urbana-Champaign, he joined the NSF-NNIN at Washington University in St. Louis as a Principal Scientist. Starting from 2011, he has been a professor of chemistry at the USTC. He has published 170 papers with over 18,000 citations (H-index 66). His research interests include

inorganic materials and devices for carbon dioxide reduction, nitrogen fixation, methane conversion, water splitting and chemical production.

## 串联反应纳米催化剂的设计：基于分步反应活性位点协调统一的氢转移反应活性提升

游洋<sup>1†</sup>, 黄浩<sup>1†</sup>, 毛可可<sup>2†</sup>, 夏松<sup>1</sup>, 武迪<sup>1</sup>, 胡灿宇<sup>1</sup>, 高超<sup>1</sup>, 刘潘一鸣<sup>1</sup>, 龙冉<sup>1\*</sup>, 武晓君<sup>1</sup>, 熊宇杰<sup>1\*</sup>

**摘要** 在一种催化纳米结构上实现高效的多步串联反应有利于提高化学转化的效率并且减少安全隐患。在确定每一个分步反应中的活性位点之后，才能够优化整个串联反应的活性。因此，确认分步反应中的活性位点是在催化纳米结构上实现高效多步串联反应的关键要素之一。在本文中，我们以氢转移反应为模型体系，展示了串联反应中分步反应的活性位点协调统一是催化剂设计中不容忽视的关键要素。我们合成了3种结构的钯纳米晶体(包括纳米立方体、八面体、四面体)，得到了不同类型的催化位点(面位点及棱角位点)，并在氢转移反应的分步反应(甲酸分解和加氢反应)中探究了不同催化位点的活性贡献程度。结果表明甲酸分解反应比较倾向于在纳米立方体的棱上和纳米八面体/四面体的面上发生，而加氢反应倾向于在3种纳米晶体的棱上发生。纳米立方体的棱位点在两个分步反应中都贡献了较大的活性，这导致了其在氢转移反应中明显具有更高的活性。即使纳米八面体/四面体在分步反应中具有相近的活性，由于串联反应的活性位点不统一，导致其在氢转移反应中的活性明显低于纳米立方体。基于以上发现，我们进一步通过提高限速步的反应速率，从而提高整个氢转移反应的活性。本工作作为合理设计串联反应中的异相纳米催化剂提供了新的思路。